ACS APPLIED POLYMER MATERIALS

pubs.acs.org/acsapm Article

Inhibitor-Sandwiched Polyelectrolyte Film for Micro/Nanopore Sealing to Enable Corrosion-Resistant Self-Healing Capability

Zhi-Hui Xie,* Wenxi Zhang, Yanqiu Li, Qiwen Yong, Liang Wu, Xiaoqiang Fan, and Chuan-Jian Zhong*

Cite This: ACS Appl. Polym. Mater. 2024, 6, 4037−4049 Read Online

ACCESS | Metrics & More | Article Recommendations | Supporting Information

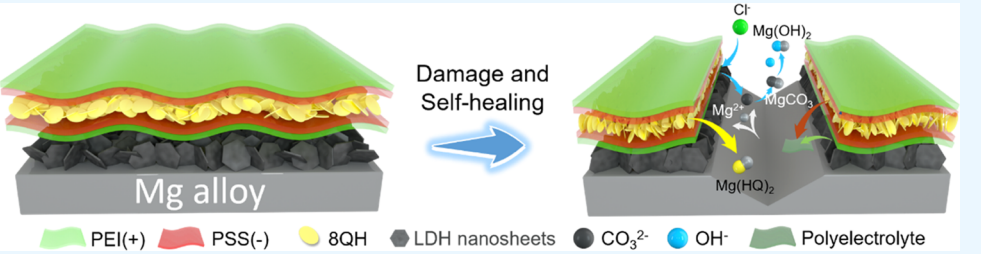

ABSTRACT: Layered double hydroxide (LDH) layers have emerged as a promising class of materials in preparing functional coatings due to their specific anion exchangeability. However, most LDH-based films exhibit micro- and nanoscale pores that are not conducive enough to block corrosive media penetration. This report demonstrates a corrosion-resistant LDH-based composite coating with an 8-hydroxyquinoline (8HQ)-sandwiched polyelectrolyte outer film. This polyelectrolyte film is flat and dense, enabling an effective pore-sealing of the LDH layer on the magnesium alloy and preventing the dissolution and diffusion of inhibitor into the bulk solution. This strategy is shown to enhance the corrosion protection performance significantly. Electrochemical measurements, including the scanning vibrating electrode technique (SVET), confirm that the as-prepared composite coating exhibits very high charge transfer resistance (~90 MΩ·cm^2), extremely low corrosion current density (<1.0 nA cm^{-2}), and superior self-healing capability. The high-performance corrosion protection is attributed to a combination of the ion-exchange capability of the LDH phase, corrosion inhibition of the 8HQ inhibitor, intrinsic properties and sealing effect of the polyelectrolyte, and decreased hydrophilicity. These findings provide insight into highly efficient sealing for porous layers on metal surfaces to achieve coating with long-term corrosion protection and self-healing capability.

KEYWORDS: *magnesium alloy, corrosion, coating, layered double hydroxide, self-healing, inhibitor*

1. INTRODUCTION

Compared with other commercial metals, magnesium alloys' merits of lightweight, high strength, and easy processing enable them to be widely applied in aerospace, automobile, and other fields.[1] However, the naturally oxidized film on the magnesium alloy surface is loose and porous. Thus, it cannot provide adequate corrosion protection.[2] Due to this significant problem, magnesium alloys must be appropriately treated before practical application.[3] Traditional approaches to prevent magnesium alloys from corrosion include electroless plating, electroplating, microarc oxidation, chemical conversion film, laser treatment, and organic coating.[4−6] However, typical protective coating usually exhibits poor durability.[7] When cracks, scratches, and other defects are produced, the coatings quickly fail, leading to rapid corrosion of the substrate, which is one of the toughest issues for practical applications.[8]

The self-healing coating has attracted much attention in various fields, including the corrosion and protection community.[9−13] Layered double hydroxides (LDHs) are new-emerged advanced materials in the self-healing coating field.[3,14] They are a class of two-dimemsional (2D) materials in the anionic clay family featuring brucite-like cationic layers with an overall positive charge to the nanosheets.[15,16] LDHs have become a hotspot of research in the surface engineering of magnesium alloys due to their unique structural characteristics.[17] For example, the corrosion inhibitor can be intercalated into the interlayer gallery of cationic layers during coating preparation through ion exchange, codeposition, and other methods.[18−20] Upon capturing the corrosive anions, inhibitors are released, which could endow the coating's physical barrier and self-healing functions and enhance the corrosion resistance. Direct adsorbing 8-hydroxyquinoline (8HQ), a green corrosion inhibitor, on the surface of the LDH phase or intercalation of 8HQ into the interlayer gallery is helpful to enhance the corrosion resistance of the LDH

Received: January 9, 2024
Revised: February 26, 2024
Accepted: March 4, 2024
Published: March 20, 2024

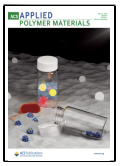

Scheme 1. Schematic Diagram Showing the Assembly of an Inhibitor-Sandwiched Polyelectrolyte to Seal the Micro/Nanopores in the LDH Layer to Form a Self-Healing Composite Coating

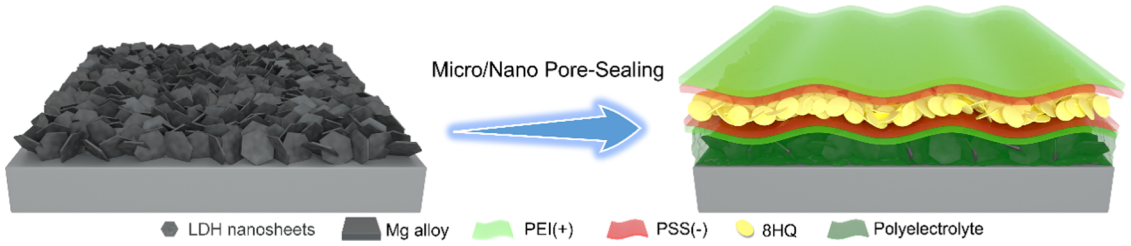

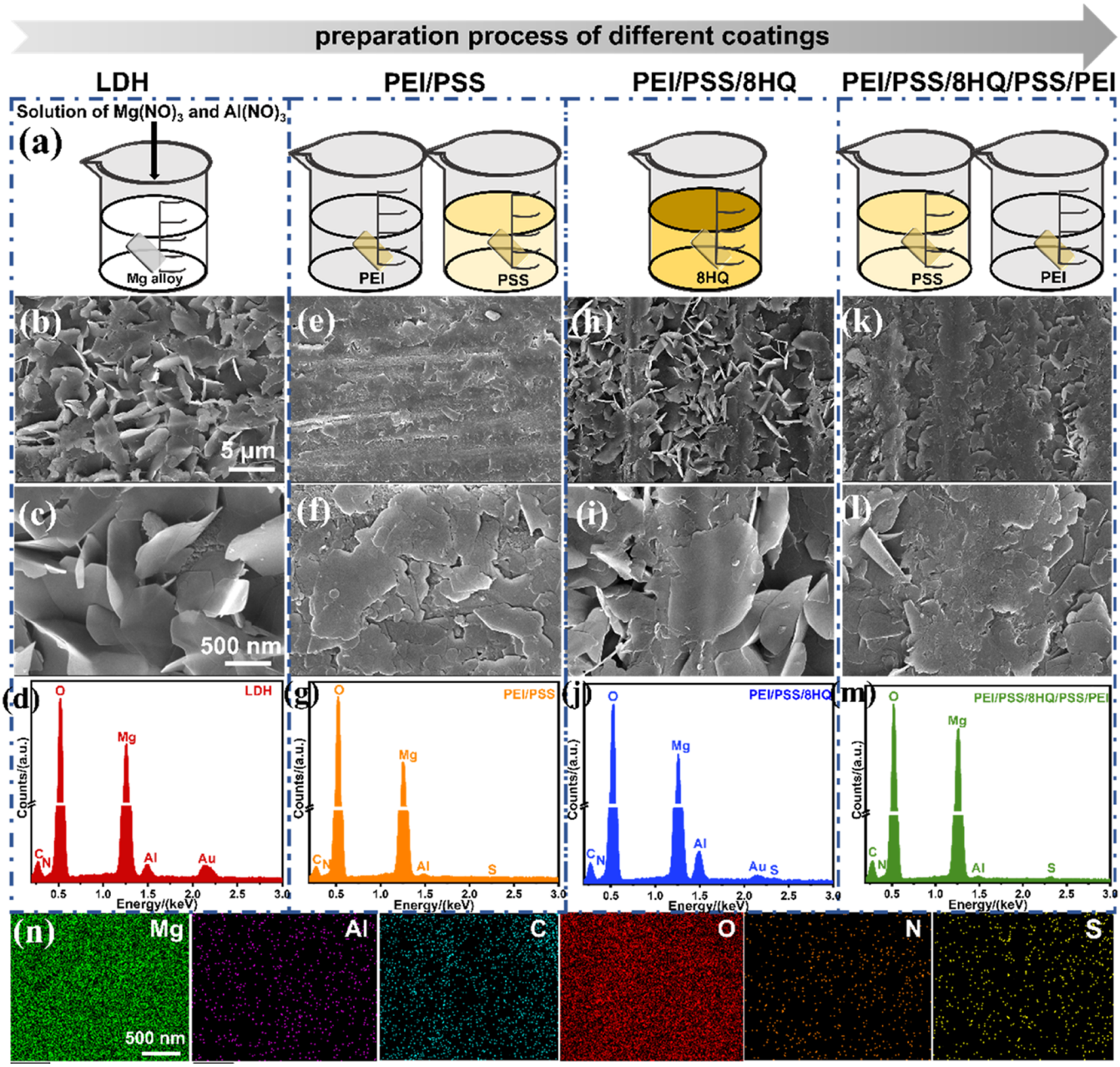

Figure 1. Surface morphology and composition: (a) schematic diagrams showing the preparation of different coatings. (b−m) SEM images and EDS spectra. (b−d) LDH, (e−g) PEI/PSS, (h−j) PEI/PSS/8HQ, and (k−m) PEI/PSS/8HQ/PSS/PEI. (n) EDS maps for PEI/PSS/8HQ/PSS/PEI coating.

film.[21] The improved corrosion resistance is attributed to the combination of 8HQ and Mg^{2+} to form a stable deposit, $Mg(HQ)_2$, which covers defects and active sites and slows down the corrosion of magnesium alloys.[22] Similarly, the LDH film allows for corrosion protection of magnesium alloys after microarc oxidation treatment with 8HQ and graphene oxide

https://doi.org/10.1021/acsapm.4c00087
ACS Appl. Polym. Mater. 2024, 6, 4037−4049

(GO).[23] However, when these 8HQ species that were intercalated into the interlayer gallery or adsorbed onto the LDH phase's surface were released, they were directly exposed to the corrosion medium. Partial 8HQ molecules spread from the magnesium alloy substrate to the bulk solution, causing corrosion inhibitor loss and reduced corrosion inhibition efficiency.[24] A GO/8HQ/PDA sandwich structure formed by reacting of GO and 8HQ, followed by polydopamine (PDA) polymerization, helps to avoid corrosion inhibitor leakage, prolongs storage of corrosion inhibitor, and enhances the corrosion protection ability of epoxy resin-based coatings.[25] Good corrosion resistance has been observed in earlier studies of layer-by-layer (LBL) self-assembly within polyelectrolyte layers via electrostatic or hydrogen bonding interactions.[26,27] For instance, poly(vinylpyrrolidone) (PVP)/poly(acrylic acid) (PAA) multilayer structure coating on the magnesium alloy surface obtained by the LBL method shows a dense and uniform physical barrier layer.[28] By covering polyethylenimine (PEI)/MXene on the surface of the inhibitors-loaded LDH phase, the physical barrier of the organic layer and the self-healing capability of the LDH phase present evident advantages, showing obviously enhanced corrosion protection for magnesium alloys.[29]

Despite the progress in exploring different coating structures, effectively sealing the microscale and nanoscale pores remains elusive. This paper demonstrates an effective strategy to construct a highly corrosion-resistant self-healing coating by inhibitor-sandwiched polyelectrolyte pore-sealing. The inhibitor-sandwiched multilayer film was assembled on the surface of an in situ-deposited MgAl-LDH layer using the LBL method (Scheme 1). The polyelectrolyte film is structurally engineered in the assembly process to seal the microscale and nanoscale pores in the LDHs layer and thus avoid the direct exposure of the inhibitor to the corrosive electrolyte, thereby reducing the leakage content to the bulk solution and increasing the inhibition efficiency. The physical barrier of the polyelectrolyte is also helpful to retard the penetration of the corrosive medium, thus achieving an intelligent coating system with long-term and efficient corrosion protection for magnesium alloys.

2. EXPERIMENTAL SECTION

2.1. Materials and Reagents. AZ31 magnesium alloy sheet (25 mm × 15 mm × 2.0 mm) contains 2.75 wt % Al, 1.15 wt % Zn, 0.16 wt % Mn, and 95.56 wt % Mg. Polyethylenimine (PEI, M_w = 70,000, 50 wt % aqueous solutions), poly(sodium 4-styrenesulfonate) (PSS, M_w = ∼700,000), 8HQ (99%), nonahydrate aluminum nitrate ($Al(NO_3)_3{\cdot}9H_2O$, ≥99%), magnesium nitrate hexahydrate ($Mg(NO_3)_2{\cdot}6H_2O$, ≥99%), and sodium chloride (NaCl, >99%) were purchased from Aladdin (Shanghai, China). Sodium hydroxide (NaOH, ≥99.9%), sodium carbonate (Na_2CO_3, ≥99.8%), and sodium phosphate (Na_3PO_4, ≥98.0%) were purchased from Sinopharm Chemical Reagent Co., Ltd. (Chengdu, China). All chemicals were used without further purification. The deionized water used in all experiments was prepared with a water purification system (UPT-II-10T, 18.2 MΩ·cm at 25 °C).

2.2. Preparation of the Polyelectrolyte-Sealed LDH Composite Coating. *2.2.1. Pretreatment of Magnesium Alloy.* To remove the oxide and grease, we polished the AZ31 magnesium alloy with 1200# sandpaper, followed by immersing it in an alkaline solution containing 50 g/L NaOH and 10 g/L Na_3PO_4 for 10 min, respectively. Afterward, the alloy sheet was washed with running deionized water and dried in hot air.

2.2.2. Preparation of the LDH Film. First, a mixed solution composed of 0.02 mol/L $Al(NO_3)_3{\cdot}9H_2O$, 0.06 mol/L $Mg(NO_3)_2{\cdot}6H_2O$, and 0.01 mol/L Na_2CO_3 was prepared. The solution was adjusted to a pH value of ∼12.0 by a NaOH solution (5.0 mol/L) and then poured into a 50 mL Teflon-lined stainless-steel autoclave. After immersing the pretreated magnesium alloy, the autoclave was sealed and placed in an oven at 125 °C for 24 h. Lastly, after washing the sheet with running deionized water and drying it at 65 °C for 24 h, the obtained sample was labeled as LDH.

2.2.3. Preparation of Polyelectrolyte-Sealed LDH Composite Coating. The inhibitor-loaded polyelectrolyte layers were assembled on the LDH surface by sequential immersing in a 2 mg/mL PEI and 2 mg/mL PSS water/ethanol (V/V = 1:1) solution for 10 min at room temperature, followed by immersing in a 10 wt % 8HQ ethanol solution for 10 min. Then, the soaking steps in PSS and PEI solutions were repeated in reverse sequence. The obtained samples are denoted by PEI/PSS/8HQ/PSS/PEI. PEI/PSS and PEI/PSS/8HQ samples were also prepared for comparison. For the PEI/PSS sample, the LDH was soaked in only PEI and PSS solutions. The PSS and PEI solution was not used after the sample was soaked in the 8HQ solution to prepare the PEI/PSS/8HQ. A schematic diagram is illustrated in Figure 1a to show the preparation process of the different coatings.

2.3. Characterization and Electrochemical Evaluation. The phase structures of the bare LDH and different polyelectrolyte-sealed LDH samples were obtained by an X-ray powder diffractometer (XRD: D8 ADVANCE, Germany). During the XRD characterization, a Cu target with a scan rate of 5° min^{-1}, scan angle of 5−80°, voltage of 40 kV, and current of 30 mA was used. Fourier transform infrared spectroscopy (FT-IR, Nicolet 6700, Thermo Scientific, Waltham, MA) was used to characterize the chemical groups of different coatings in the wavenumber range 500−4000 cm^{-1}. The coatings' elemental composition and chemical state were analyzed by an X-ray photoelectron spectroscopy (XPS, 250Xi). The acquired XPS data were calibrated using the binding energy of adventitious carbon (C 1s: 284.8 eV) and then fitted with XPSPeak software. A scanning electron microscope (SEM, Hitachi SU8020) coupling with an energy dispersive spectrometer (EDS) was used to observe the different coatings' surface morphology and elemental distribution. The wettability of the sample was evaluated by measuring the static contact angle (CA) using an optical contact angle meter (SL200 KS) after dropping a water droplet with a volume of 5.0 μL at the coating surface at 25 °C. A cross-cut method is used to test the adhesion between the coating and the substrate based on the standard of GB/T9286−88.

A three-electrode system, including the working electrode (exposed area 1.0 cm^2), was immersed in a 3.5 wt % NaCl solution and tested at room temperature (∼25 °C) using an electrochemical workstation (Gamry) to evaluate the corrosion resistance. The other two electrodes of the three-electrode system were the reference electrode (saturated calomel electrode (SCE)) and the counter electrode (platinum sheet). The three-electrode system was placed in a Faraday cage to isolate the coating sample from external electromagnetic radiation. Before electrochemical impedance spectroscopy (EIS) and Tafel curves testing, open circuit potential (OCP) vs time curves were measured for at least 1200 s until a relatively stable OCP was obtained. Due to the huge impedance, EIS diagrams were acquired in the 10^5 to 10^{-2} Hz frequency range with an amplitude of 25 mV. The Tafel tests were conducted at a scan rate of 1.0 mV s^{-1} and over a potential range of −500−500 mV (vs OCP).[30] The corrosion current density (j_{corr}) values were obtained by fitting the Tafel curves and were used to calculate the corrosion protection efficiency (η) based on the following equation

$$\eta = \frac{j'_{corr} - j_{corr}}{j'_{corr}} \times 100\% \quad (1)$$

where j'_{corr} and j_{corr} represent the corrosion current densities of bare magnesium alloy and magnesium alloy with different coatings, respectively. The electrochemical parameters associated with the EIS and Tafel curves were fitted by using Gamry Analyst software.

https://doi.org/10.1021/acsapm.4c00087
ACS Appl. Polym. Mater. 2024, 6, 4037−4049

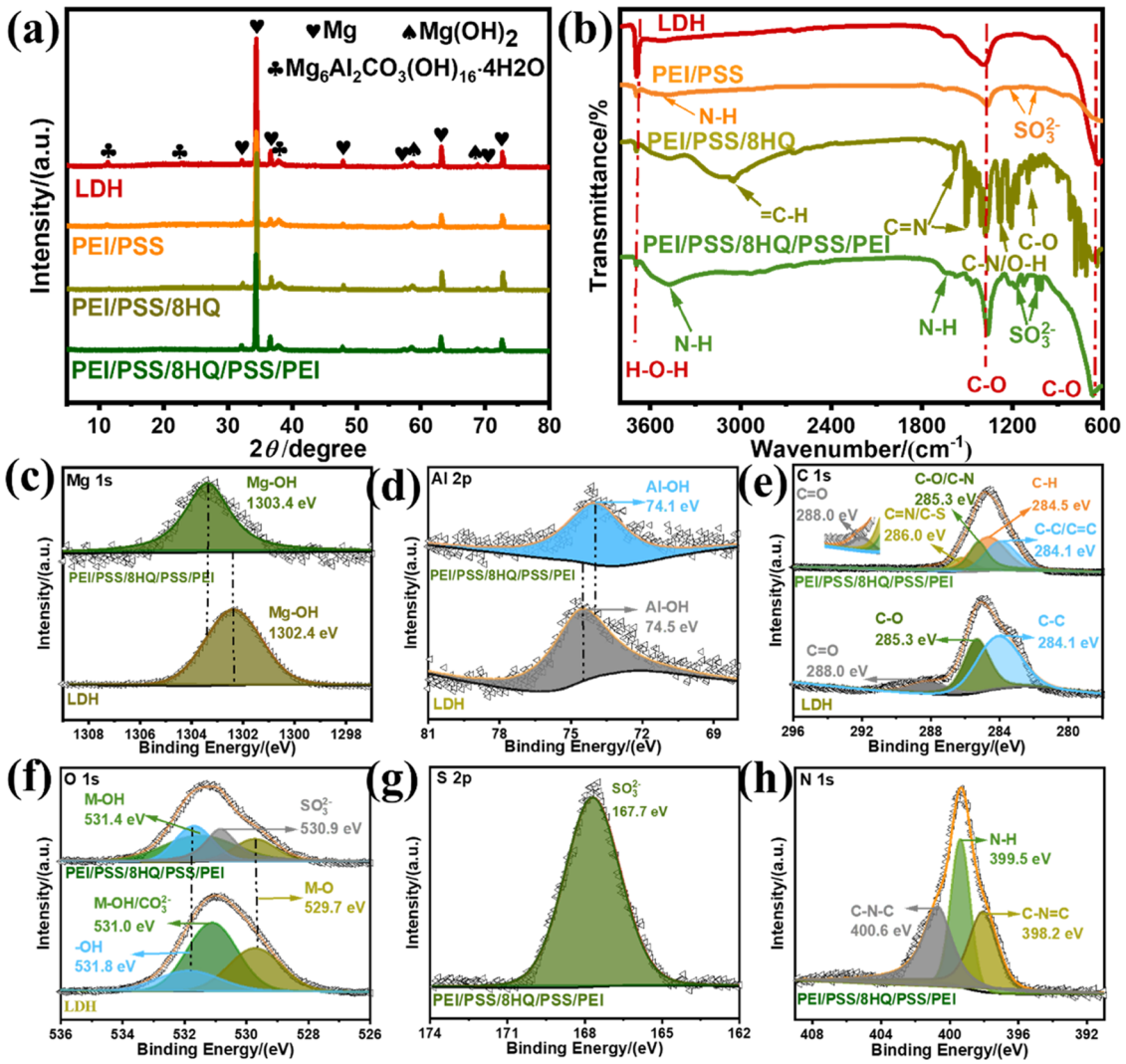

Figure 2. Different films and surface structures: (a) XRD patterns and (b) FT-IR spectra of LDH, PEI/PSS, PEI/PSS/8HQ, and PEI/PSS/8HQ/PSS/PEI coatings on the Mg alloy surface. High-resolution XPS spectra of (c) Mg 1s, (d) Al 2p, (e) C 1s, (f) O 1s, (g) S 2p, and (h) N 1s for single LDH and composite PEI/PSS/8HQ/PSS/PEI coatings.

The electrochemical tests for each sample were performed more than three times to ensure reproducibility and reliability.

The current density of the coating surface was monitored using a scanning vibrating electrode technique (SVET, Applicable Electronics, PSDA-2, Science Wares, Inc., Falmouth, MA) to examine the self-healing properties of the coating. Before testing, the samples were wrapped with edible wax and fixed on an epoxy resin substrate to expose the same area of the coating surface and introduce a defect of approximately 76 μm in diameter in the exposed area. The current signal was collected by using a Pr−Ir microelectrode scanning vibration probe (with a black platinum sphere tip, 20 μm in diameter) placed 150 μm above the sample surface. The widths and changes of the scratch defects of the different coatings before and after the immersion experiments and the needle cone defects before and after the SVET tests were observed by using a metallographic microscope (IE500M, China).

3. RESULTS AND DISCUSSION

3.1. Morphology, Composition, and Structure. The evolution of surface morphology and composition of LDH coatings with polyelectrolyte modification was first examined by SEM and EDS techniques (Figure 1). The LDH coating on the Mg surface derived by the hydrothermal method consists of many irregular nanoflakes perpendicular to the substrate (Figure 1b−c), consistent with the morphology of LDH phases.[31−33] Compared with a single LDH film, the PEI/PSS film surface is denser without evident gaps (Figure 1e). The high-magnification image (Figure 1f) shows that the flakes adsorbed on the LDH surface display an orientation parallel to that of the substrate. This type of structure presents a layer to retard the penetration of corrosive ions into the underlying matrix. When the corrosion inhibitor 8HQ was adsorbed onto the PEI/PSS film, a flake structure perpendicular to the substrate appeared again (Figure 1h−i), similar to those reported for 8HQ adsorbed directly on the LDH surface.[21] The surface morphologies of the PEI/PSS/8HQ/PSS/PEI coatings (Figure 1k−l) are similar to those of the PEI/PSS (Figure 1e−f). The surface is relatively dense and flat without the apparent porous structure of perpendicularly grown nanosheets, indicating the successful coverage of the polyelectrolyte film on the underlying 8HQ layer. Moreover, the elemental compositions were analyzed (Figures 1d−m,1j, and S1). Compared with single LDH coatings, the Mg, Al, C, and O elements were detected. After depositing polyelectrolyte and loading inhibitor, S and N elements were detected, where S came from the adsorbed PSS and N came from the PEI and

https://doi.org/10.1021/acsapm.4c00087
ACS Appl. Polym. Mater. 2024, 6, 4037−4049

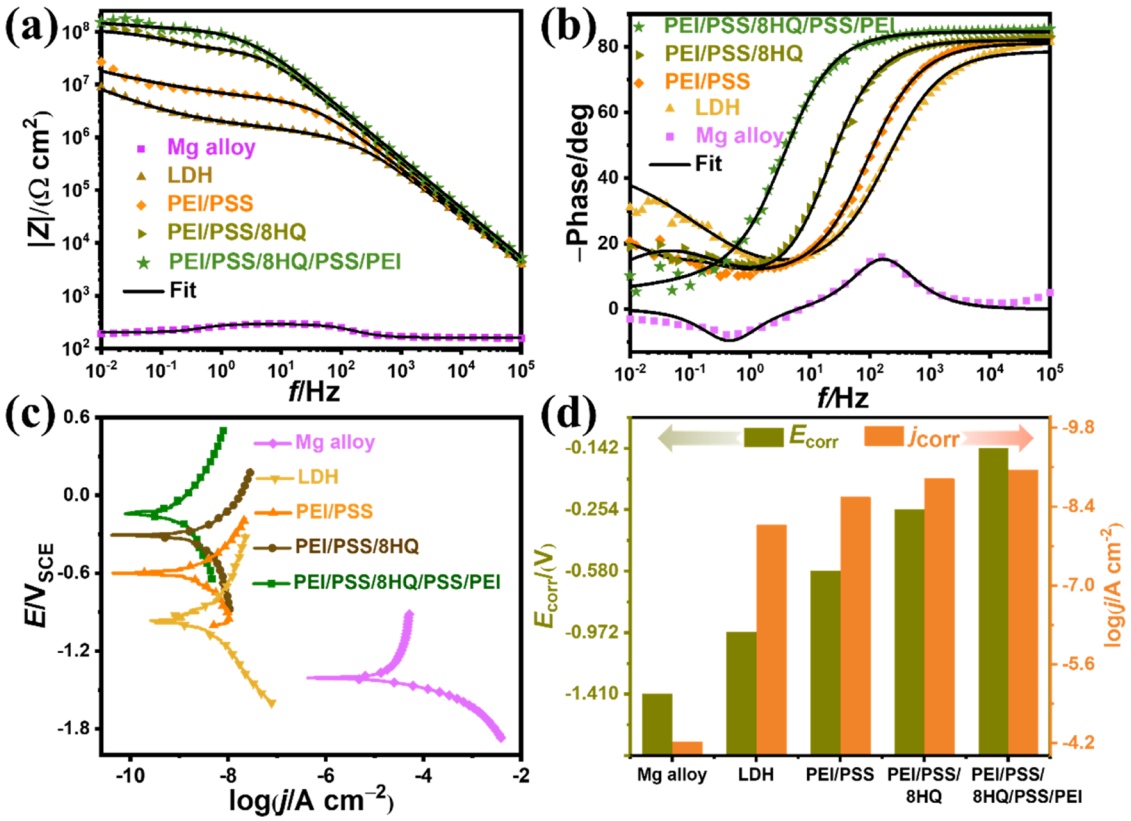

Figure 3. Electrochemical characteristics: (a) Bode magnitude and (b) Bode phase plots of bare Mg alloy and Mg alloys with LDH, PEI/PSS, PEI/PSS/8HQ, and PEI/PSS/8HQ/PSS/PEI overlayers in 3.5 wt % NaCl solutions at room temperature. (c) Tafel curves and (d) corresponding column diagrams of E_{corr} and j_{corr} of bare Mg alloy and different coatings on the Mg alloy surface.

8HQ. Based on the percentages of different elements in the four coatings (Table S1), the contents of C, N, and S elements increase with the stepwise adsorption of the polyelectrolyte and inhibitor, indicating that the organic PEI, PSS, and 8HQ were successfully assembled layer-by-layer on the LDH film's surface. The composite polyelectrolyte film was self-assembled by ionic bonds between the positively charged PEI and negatively charged PSS. The corrosion inhibitor 8HQ was entrapped into the nanonetwork of the multilayers as a dopant or a component of the polyelectrolyte.[34]

In addition to the strong diffraction peaks originating from the substrate magnesium at 2θ equal to 32.5, 34.6, 47.2, 57.8, 63.6, 69.2, and 73.0° (JCPDS No. 35−0821), a weak diffraction peak attributing to $Mg(OH)_2$ (JCPDS No. 41−1428) was observed at 59.0° after growing the LDH film on the magnesium alloy (Figure 2a). More importantly, distinctive peaks attributed to the LDH phase were observed at 11.7, 23.2, and 38.3° (JCPDS No. 14−0525), indicating the successful formation of good crystalline LDH phase on the magnesium alloy surface. With the LBL assembly of the polyelectrolyte, the organic coating thickness gradually increased and weakened X-ray penetration. The intensity of the characteristic peaks belonging to the LDH phase at 11.7 and 23.2° gradually declined and even disappeared, further proving the adsorption of the polyelectrolyte on the LDH phase's surface.

The four coatings on Mg surfaces showed evident absorption peaks at 3689 cm^{-1} in FT-IR spectra corresponding to the stretching vibration of the intercalated water molecules in the LDH phase (Figure 2b).[35] The absorption bands at 1386 and 637 cm^{-1} are associated with the asymmetric stretching vibrations resulting from the intercalated carbonate ion (CO_3^{2-}) in the LDH phase. The weak absorption peaks in the low wavenumber range are attributed to lattice vibrations of the M−O (M = Mg, Al) bonds.[36] For the LDH/PEI/PSS sample, the absorption peaks at wavenumbers 1184 and 1042 cm^{-1} correspond to symmetric and asymmetric vibrations from the sulfonate (SO_3^{2-}) in the anionic polyelectrolyte (i.e., PSS), respectively.[37] The absorption band at 3440 cm^{-1} is attributed to N−H bonding (NH) in the cationic polyelectrolyte (i.e., PEI). After treatment in an 8HQ solution, the sample shows more new absorption peaks, including the stretching vibrations of C−N/O−H bonds at 1280 cm^{-1}, C−O (C−OH) bonds at 1093 cm^{-1}, C−H bond at 3065 cm^{-1}, and C═N bond at 1571 and 1630 cm^{-1}.[25,38,39] All of the peaks are related to the 8HQ structure, indicating the successful loading of 8HQ on the polyelectrolyte film. In the FT-IR spectrum of the PEI/PSS/8HQ/PSS/PEI coating, the absorption peaks originating from the N−H bond in the PEI (3440 cm^{-1}) and SO_3^{2-} in the PSS (1184 and 1042 cm^{-1}) were significantly increased in intensity due to the further adsorption of polyelectrolyte on the surface. These results indicate the successful assembly of PEI and PSS polyelectrolytes and the loading of 8HQ inhibitors on the LDH phase surface.

The XPS high-resolution spectra of Mg 1s and Al 2p of LDH and PEI/PSS/8HQ/PSS/PEI coatings show that the binding energy of the Mg−O bond increased by 1.0 from 1302.4 to 1303.4 eV and that of the Al−O bond decreased by 0.4 from 74.5 to 74.1 eV after polyelectrolyte adsorption on the LDH phase (Figure 2c−d). The binding energy shifts indicate that chemisorption processes were involved during forming polyelectrolyte films and loading 8HQ inhibitor.[40,41] Based on the C 1s high-resolution XPS spectra for LDH and PEI/

https://doi.org/10.1021/acsapm.4c00087
ACS Appl. Polym. Mater. 2024, 6, 4037−4049

PSS/8HQ/PSS/PEI coatings, it can be seen that the C 1s spectrum of LDH includes the peak of contaminated carbon at 284.1 eV, the peaks of the C−O single bond (285.3 eV) and the C═O double bond (288.0 eV) in CO_3^{2-} (bottom curves in Figure 2e). By comparison, the C 1s spectrum of the PEI/PSS/8HQ/PSS/PEI layer shows new characteristic peaks of C−S/C═N (286.0 eV) and C−H (284.5 eV).[42−44] These newly emerged peaks result from the adsorbed PEI and PSS polyelectrolytes and 8HQ inhibitors on the LDH surface (top curves in Figure 2e). Although C−N bonds exist in PEI and 8HQ, it is impossible to distinguish the C−N and C−O bonds in the C 1s spectrum because they have the same characteristic peak position (285.3 eV). Similarly, it is also difficult to distinguish the C═C double bonds and C−C single bonds in the PSS and 8HQ. The O 1s high-resolution XPS spectrum of the single LDH film (bottom of Figure 2f) is fitted to three peaks, namely, the peak with a binding energy of 531.8 eV for −OH, 531.0 eV for M−OH/CO_3^{2-}, and 529.7 eV for M−O (M = Mg, Al) bonds. After depositing the PEI/PSS/8HQ/PSS/PEI layer (top of Figure 2f), the binding energy of M−OH increases by 0.4 to 531.4 eV, further demonstrating the bonding of the −OH group from the LDH phase with the polyelectrolyte, in agreement with the results of Mg 1s and Al 2p high-resolution XPS spectra. Besides, a characteristic peak for SO_3^{2-} in PSS is observed at a binding energy of 530.9 eV,[45] confirmed by the S 2p high-resolution XPS spectrum (167.7 eV, Figure 2g). In the N 1s high-resolution XPS spectrum (Figure 2h), the two characteristic peaks for the N−H (399.5 eV) and C−N−C (400.6 eV) bonds result from the PEI polyelectrolyte. The characteristic peak for C−N═C (398.2 eV) is attributed to the 8HQ inhibitor.[46] The XPS results further consolidate the successful deposition of an inhibitor-loaded polyelectrolyte film on the LDH layer. Owing to the rich −OH groups on the surface of the LDH phase and the N−H bond in the PEI film, N−H···O-type hydrogen bonds can be formed successfully,[37,47] which is expected to improve the adhesion and is confirmed by the tape test method (Figure S2).

3.2. Anticorrosion and Self-Healing Characteristics.

The high-frequency, middle-frequency, and low-frequency regions of the EIS spectrum reflect the outer, inner, and substrate/coating interface properties of the coating.[19,48,49] Compared to the bare magnesium alloy, the impedance values of the substrate with different coatings show a substantial increase in the whole frequency range (Figure 3). Compared with the single LDH film, the impedance values of the coatings with polyelectrolyte layers show different degrees of enhancement in the low-frequency region (Figure 3a). Especially after 8HQ adsorption, the coating offers the most significant enhancement in impedance values in the low-frequency range. This variation in impedance indicates that the corrosion protection of the inhibitor-loaded composite coating is mainly attributed to the inhibition of the 8HQ inhibitor and the physical barrier of the polyelectrolyte film. The density of the coating can also be determined qualitatively by the phase angle value in the high-frequency region. The closer the phase angle in the high-frequency region is to 90°, the denser the coating and the better the corrosion resistance is.[33] Figure 3b shows that the high-frequency phase angle of bare magnesium alloy is close to 0°, meaning that the denseness of the naturally oxidized film on the magnesium alloy surface is very poor, making its corrosion protection ability unacceptable. The high-frequency phase angles of LDH, PEI/PSS, PEI/PSS/8HQ, and especially PEI/PSS/8HQ/PSS/PEI coatings decrease sequentially and finally reach −87° at a frequency of 10 kHz, indicating that the polyelectrolyte deposition and inhibitor loading significantly enhance the dense and corrosion protection performance of the LDH-based composite coatings.

In addition to the qualitative comparison described above, equivalent circuit (EC) models were used to fit EIS spectra and quantitatively compare the corrosion resistances of different coatings. The EC models of the LDH and polyelectrolyte-(PEMu) modified LDH coatings are shown in Figure S3a,b, where R_s represents the solution resistance, CPE_{LDH} and R_{LDH} represent the constant phase element and resistance of the LDH layer, respectively, CPE_{dl}, and R_{ct} represent the constant phase angle element and charge transfer resistance of the double electric layer, respectively, and Z_w represents the Warburg diffusion impedance, which indicates the ion-exchange interaction in the LDH phase.[21] Compared with the single LDH layer, the new CPE_{PEMu} and R_{PEMu} in Figure S3b represent the different electrolyte layers' constant phase element and resistance. The fitted electrochemical parameters for different coatings are listed in Table S2. The R_{ct} value of bare magnesium alloy is only 318 Ω·cm^2 in a 3.5 wt % NaCl solution because of its poor corrosion resistance and occurrence of severe corrosion at the surface.[50] Due to the physical barrier and ion-exchange capability of the LDH layer, the R_{ct} value of the magnesium alloy after growing the LDH phase jumps to 1.15 MΩ·cm^2, indicating a significant increase in corrosion resistance. After treatment of LDH with PEI/PSS, the R_{ct} value of the coating increases more than 3 times its original value, reaching 3.57 MΩ·cm^2, attributed to the physical barrier of the polyelectrolyte layer. After loading the 8HQ inhibitor, the R_{ct} value of the obtained PEI/PSS/8HQ coating increases almost 20 times to 68.00 MΩ·cm^2, mainly attributed to the excellent inhibition of the 8HQ inhibitor. To prevent the ineffective diffusion of inhibitor into the bulk solution and enhance the inhibition efficiency, the PSS/PEI layer was deposited by electrostatic deposition. The R_{ct} value of the obtained PEI/PSS/8HQ/PSS/PEI coating further increases to 86.8 MΩ·cm^2, which is again attributed to the physical barrier of the polyelectrolyte film. Briefly, the PEI/PSS/8HQ/PSS/PEI coatings exert the polyelectrolyte film's physical barrier effect to seal the pores in the LDH layer and efficiently utilize the inhibition of the 8HQ inhibitor, showing high-performance corrosion protection.

The results of Tafel curves also indicate the excellent corrosion protection of the PEI/PSS/8HQ/PSS/PEI coating for the magnesium alloy (Figure 3c). Compared with bare magnesium alloy, the coatings' corrosion potentials (E_{corr}) shift significantly toward a more positive direction, and the j_{corr} decreases notably. Generally, a more positive E_{corr} of the coating indicates better corrosion protection.[51] The bare magnesium alloy shows the most negative E_{corr} (1410 mV) and the highest j_{corr} (6.0×10^{-5} A cm^{-2}) among these samples (Figure 3d and Table S3). The LDH layer presents a relatively positive E_{corr} (972 mV) and a small j_{corr} (8.37 nA cm^{-2}), indicating a notable enhancement against corrosion. Compared to the single LDH layer, after depositing the PEI/PSS/8HQ/PSS/8HQ film, the formed composite coating exhibits the most positive E_{corr} (−142 mV) and the lowest j_{corr} (0.888 nA cm^{-2}). The corrosion protection efficiency of the composite coating reaches 99.999%, indicating excellent corrosion protection of the coating for magnesium alloy.

https://doi.org/10.1021/acsapm.4c00087
ACS Appl. Polym. Mater. 2024, 6, 4037−4049

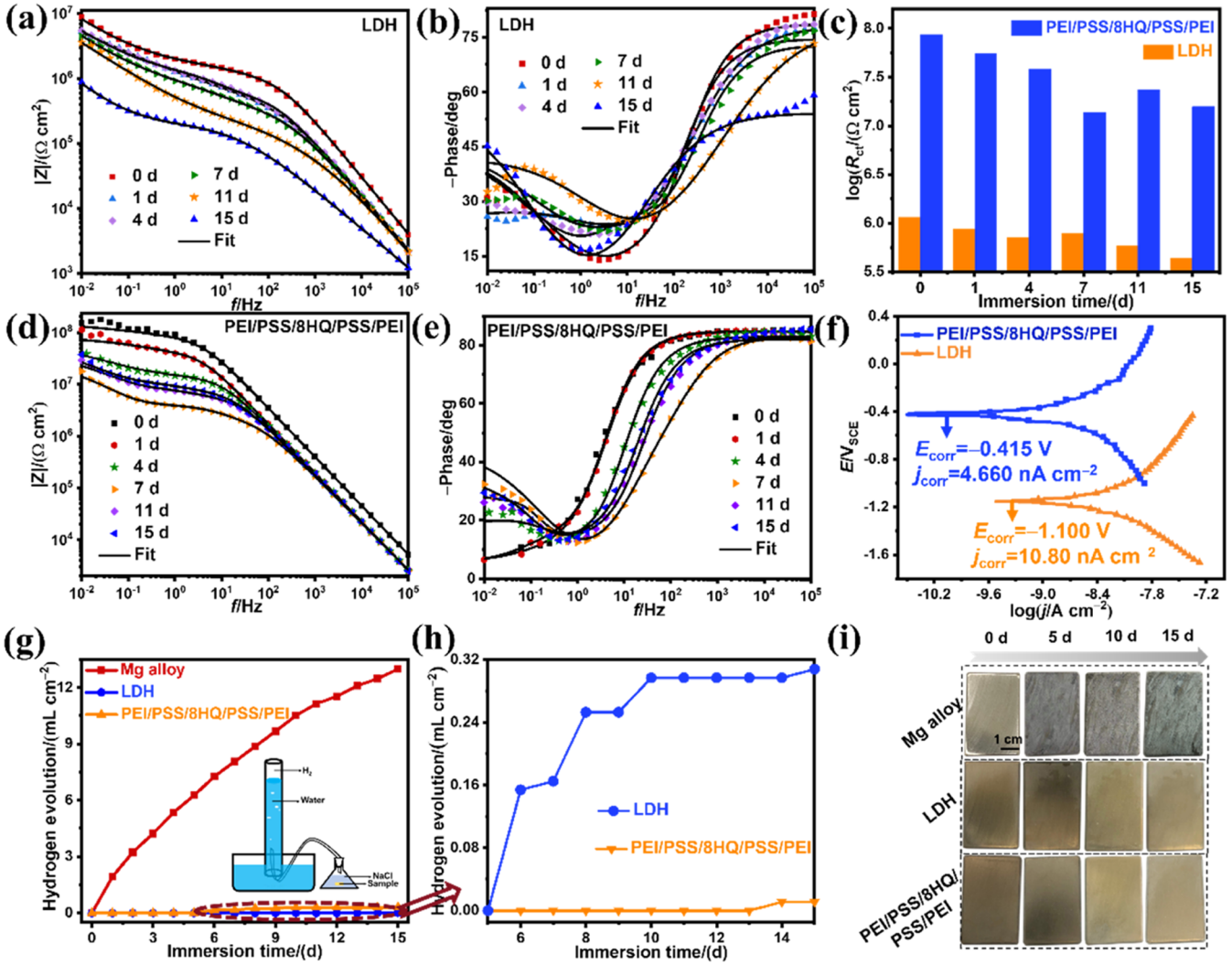

Figure 4. Evolution of the electrochemical characteristics: (a−d) Bode diagrams of (a, b) LDH and (c, d) PEI/PSS/8HQ/PSS/PEI coatings with soaking days in 3.5 wt % NaCl solutions, (e) log R_{ct} values over time, and (f) Tafel curve after exposure for 15 days. (g, h) Hydrogen evolution experiment of the Mg alloy (25 × 15 × 2 mm^3) with and without LDH and PEI/PSS/8HQ/PSS/PEI coatings after immersing in 50 mL of NaCl solutions for half a month. (i) Digital pictures of the macroscopic morphologies of the samples after exposure to corrosive solutions for different days.

The EIS and Tafel plots were also employed to compare the long-lasting corrosion protection performance of the LDH and PEI/PSS/8HQ/PSS/PEI coatings during 15 days of exposure to corrosive solutions (Figure 4 and Table S4). Although the R_{ct} value of the LDH coating slowly decreases with increasing soaking time, it remains above 0.43 MΩ·cm^2 after 15 days of soaking, mainly attributed to the sound physical barrier and ion-exchange function of the LDH layer. In contrast, the R_{ct} value of the PEI/PSS/8HQ/PSS/PEI coating is 15.69 MΩ·cm^2 after the same period of immersion (Figure 4c,e and Table S4), which is about 36 times that of the LDH coating. Moreover, the PEI/PSS/8HQ/PSS/PEI coating displays an evident increase in the R_{ct} value up to 11 days of immersion, which may be related to the release of inhibitors. In addition, the absolute value of the phase angle at high-frequency (10 kHz) for the LDH coating gradually decreases from 80 to 60° as the soaking time increases (Figure 4b). This decrease in impedance results from the gradual degradation of the LDH layer during the soaking process.[52,53] As for the PEI/PSS/8HQ/PSS/PEI coating, after experiencing the same soaking time, the absolute value of the phase angle only decreases from 87 to 80°, indicating better corrosion resistance compared to the single LDH layer (Figure 4d). From the Tafel curves (Figure 4f), the corrosion potentials of PEI/PSS/8HQ/PSS/PEI and LDH coatings after 15 days of immersion are −0.415 and −1.100 V and the corrosion current densities are 4.66 and 10.80 nA cm^{-2}, respectively. Compared with the single LDH layer, the PEI/PSS/8HQ/PSS/PEI composite coating still exhibits a significantly larger R_{ct} value, more positive E_{corr}, and lower j_{corr} even after long-time immersion in the corrosive medium, suggesting stable corrosion protection performance.

The superior long-term corrosion resistance of the PEI/PSS/8HQ/PSS/PEI coating is also demonstrated by hydrogen evolution experiments using a buret closed at one end (inset in Figure 4g). The bare magnesium alloy exhibits a huge hydrogen volume during exposure (Figure 4h). Although the hydrogen volumes for both coatings are tiny throughout the soaking period, the amount of hydrogen is only 0.01 mL cm^{-2} for the PEI/PSS/8HQ/PSS/PSS/8HQ coating after 15 days of soaking, which is significantly lower than that for the single LDH layer (0.31 mL cm^{-2}). After 5 days of immersion, the bare magnesium alloy was corroded seriously, and the surface

https://doi.org/10.1021/acsapm.4c00087
ACS Appl. Polym. Mater. 2024, 6, 4037−4049

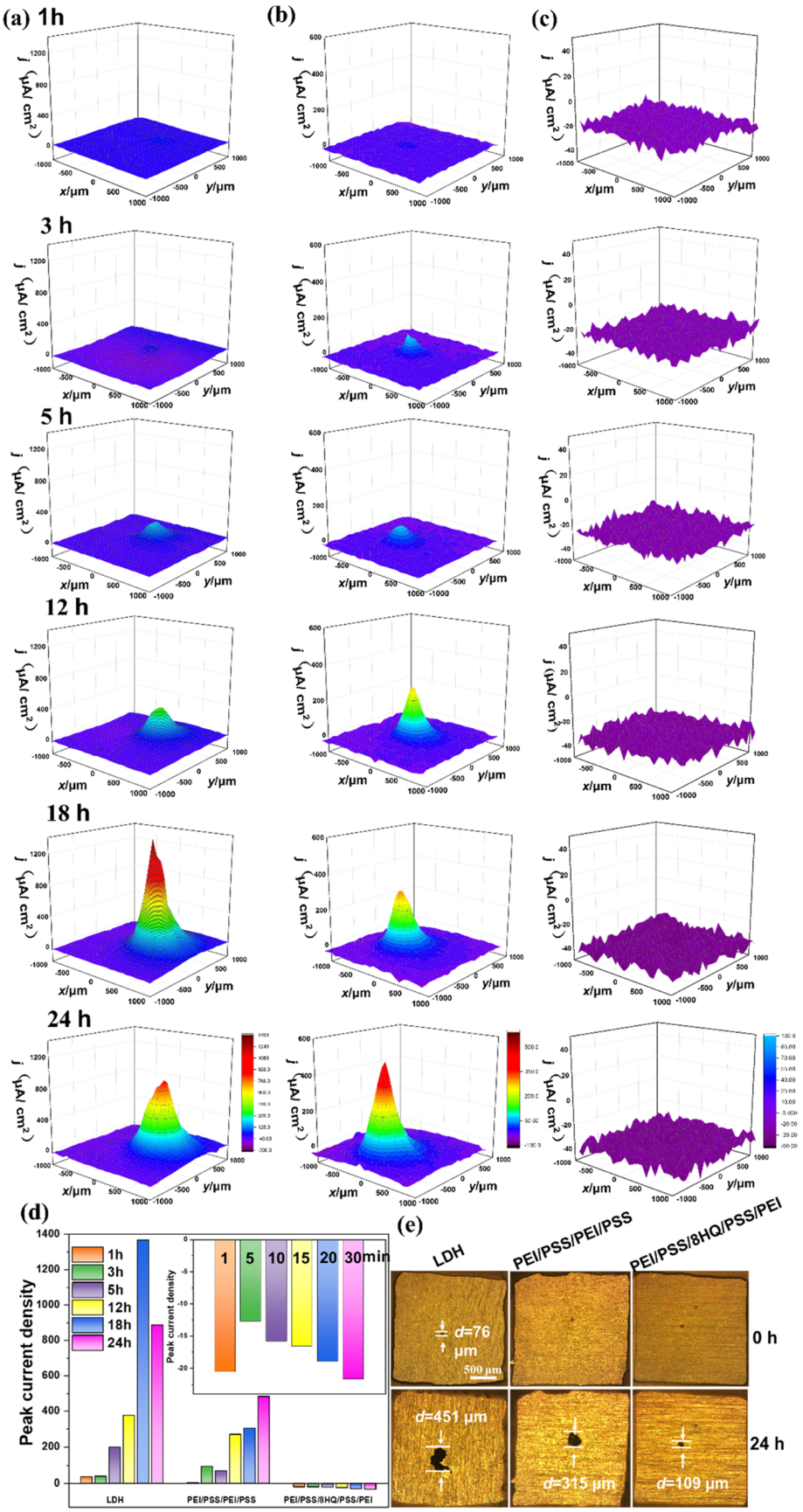

Figure 5. 3D SVET current density plots: (a) LDH, (b) PEI/PSS/PEI/PSS, and (c) PEI/PSS/8HQ/PSS/PEI coatings on the magnesium alloy surface at different exposure times in corrosive media. (d) Variations of peak current densities with different immersion times at artificial defects for the three coatings based on the 3D SVET maps and (e) corresponding metallographs before and after SVET testing in 3.5 wt % NaCl solutions for 24 h, showing the self-healing processes and demonstrating the superior corrosion protection of the as-obtained composite coating.

https://doi.org/10.1021/acsapm.4c00087
ACS Appl. Polym. Mater. 2024, 6, 4037−4049

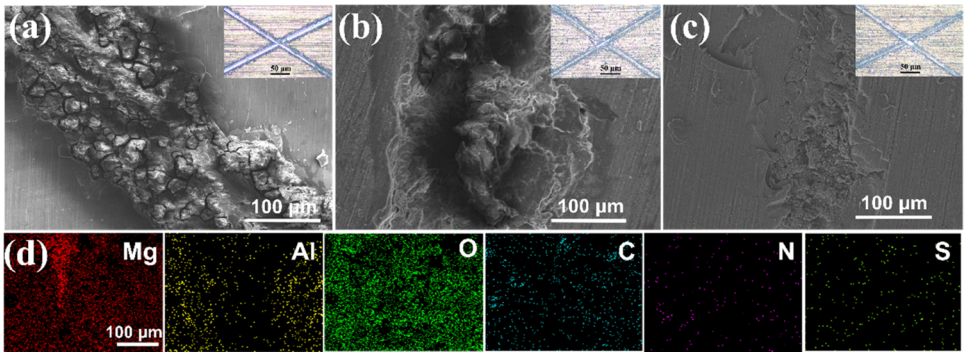

Figure 6. Morphologies and compositions of the coatings and artificial scratches: (a–c) SEM images for (a) LDH, (b) PEI/PSS/PEI/PSS, and (c) PEI/PSS/8HQ/PSS/PEI coatings after 24 h immersion and metallographic images of scratches before immersion in corrosive media (insets). (d) EDS maps of the PEI/PSS/8HQ/PSS/PEI coating around the scratched areas after exposure to corrosive media.

was entirely covered by corrosion products (Figure 4i). By contrast, after 15 days of immersion, the visual appearances of the LDH and PEI/PSS/8HQ/PSS/PSS coatings were similar to those before immersion without obvious corrosion signs. The hydrogen evolution results and digital pictures demonstrate the relatively stable corrosion resistance of the LDH and PEI/PSS/8HQ/PSS/PSS/8HQ coatings. However, the corrosion resistance of the PEI/PSS/8HQ/PSS/PEI coating is better than that of the single LDH coating. This improvement in corrosion protection is doubtlessly related to the inhibitor's inhibition and the physical barrier of the polyelectrolyte film.

The cathodic and anodic behaviors at the artificial microdefects were analyzed by measuring the current densities on different coating surfaces using an SVET method (Figure 5). Obvious anodic behavior is observed when the magnesium alloy with pure LDH coating is immersed in a 3.5 wt % NaCl solution (Figure 5a,d). In the early immersion stage, the corrosion current density increases with the immersion time. After 18 h of immersion, the current density at the defects decreases, probably because the self-healing effect of the LDH phase and the accumulation of corrosion products at the defects have a certain inhibitory effect on corrosion.[54] The current density variation of the PEI/PSS/PEI/PSS coating in the corrosive medium is similar to that of the LDH coating (Figure 5b), which also tends to increase and decrease in current density with increasing time. However, compared to the single LDH coating, the PEI/PSS/PEI/PSS coating shows a slight decrease in current density after only 3 h of exposure. The time required for the latter to undergo self-healing is significantly reduced, indicating improved corrosion protection due to the mobility of the polyelectrolyte.[55] The corrosion current density increases significantly again with increasing immersion time, indicating that the anodic process was not sufficiently inhibited. However, the maximum corrosion current density of the PEI/PSS/PEI/PSS coating is remarkably reduced to about 482.5 μA cm^{-2} after 24 h of immersion, which is only one-third that of the single LDH coating. In contrast, the PEI/PSS/8HQ/PSS/PEI coatings exhibit significantly different current density variations during the 24 h immersion (Figure 5c,d). Evident anodic currents are not examined within the immersion experiment, indicating sufficient inhibition of the anodic oxidation reactions. The current density variation of the PEI/PSS/8HQ/PSS/PEI coatings within 30 min (Figure S4) further demonstrates that 8HQ, as a mix-type inhibitor, adequately inhibits the anodic reaction in a very short period while restraining the cathodic reaction in a very slow rate.[21] The cathodic current density mainly originates from the reduction reaction of water to hydrogen gas.[56] The cathodic current density is slightly higher than 30 μA cm^{-2} at the beginning (1 min) and was suppressed and decreased to about 15 μA cm^{-2} after 5.0 min due to the continuous release of the 8HQ inhibitor. Subsequently, although the current density increases slowly with time, it increases to only about 30 μA cm^{-2} after 30 min. The initial diameters of the artificial defects at the surfaces of the three coatings are all ~76 μm (Figure 5e). After 24 h of exposure, the sizes of the defects at the LDH and PEI/PSS/PEI/PSS coatings' surfaces increase notably to around 451 and 315 μm, respectively. In contrast, the increased dimension of the defects in the case of the PEI/PSS/8HQ/PSS/PEI coating is much smaller. The SVET and metallographic images further demonstrate the good self-healing ability and corrosion resistance of the PEI/PSS/8HQ/PSS/PEI coating.

The LDH, PEI/PSS/PEI/PSS, and PEI/PSS/8HQ/PSS/PEI coatings with artificial scratches were immersed in 3.5 wt % NaCl solutions. The metal surface's corrosion extent and elemental changes were observed (Figure 6a–c). The metallographic images show that the initial scratches of the three coatings were deep to the substrate and similar in width. After immersion in the corrosive medium, the depths of the scratches on the surfaces of the three coatings were less noticeable. The cuts become shallow because of the chemical reactions near the scratches during immersion and the formation of deposits to fill the defects. However, the sediments in the scratch area of the pure LDH and PEI/PSS/PEI/PSS coatings are loose, especially the former, which exhibits obvious microcracks in the precipitation film at the scratch area. The reason is that in this case, the corrosion medium penetrated the magnesium alloy and the sediment film was composed of loose and porous magnesium hydroxide and magnesium oxide. In contrast, the precipitation layer at the scratch area of the PEI/PSS/8HQ/PSS/PEI coating is very flat and dense. The EDS results show that, compared to the PEI/PSS/PSS/PEI coating, the PEI/PSS/8HQ/PSS/PEI coating exhibits notably higher content for N element in the scratch area (Figure 6d and Table S5), confirming the presence of 8HQ inhibitor at the scratched region in the latter.

3.3. Self-Healing Mechanism of the Polyelectrolyte-Modified Coating. The superior corrosion resistance of the as-prepared multilayer (PEI/PSS/8HQ/PSS/PEI) composite coating suggests a self-healing function. The function stems from a combination of the ion-exchange capability of the LDH

https://doi.org/10.1021/acsapm.4c00087
ACS Appl. Polym. Mater. 2024, 6, 4037–4049

Scheme 2. Schematic Illustration of the Self-Healing Mechanism for the PEI/PSS/8HQ/PSS/PEI Coating on the Mg Alloy

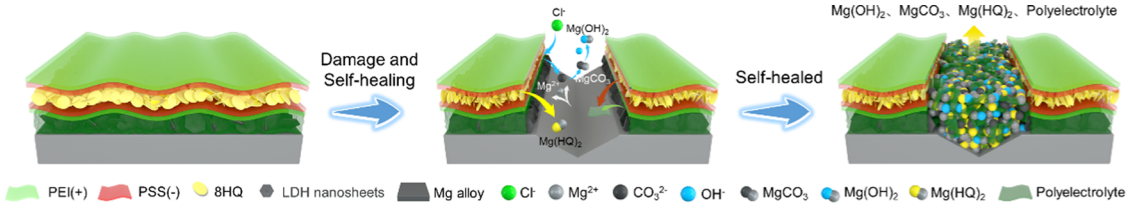

phase, the inhibition of the 8HQ inhibitor, and the sealing effect of the polyelectrolyte on the porous structures.

First, the physical barrier and anion exchangeability of the LDH layer are crucial factors in the self-healing function. In addition to acting as a physical barrier, the ion-exchange property of the LDH phase is also important because when mechanical or chemical damage occurs, the LDH phase can capture corrosive anions (e.g., Cl^-) and release inhibitors to inhibit the corrosion. Typically, the CO_3^{2-} intercalated LDH phase is less likely to undergo ion exchange with other anions. However, the CO_3^{2-} intercalated LDH phase deposited on magnesium alloys undergoes ion exchange. The ion exchange does not affect the structure when immersed in a NaCl solution for a long time[57] because CO_3^{2-} ions react with Mg^{2+} to produce $MgCO_3$ precipitate, which promotes the exchange reaction between CO_3^{2-} and Cl^- ions. Moreover, owing to the relatively high solubility product constant of $MgCO_3$, it is easily transformed to $Mg(OH)_2$ precipitation at the corrosion defects, hindering further corrosion.

Second, a dense and corrosion-resistant $Mg(HQ)_2$ film is formed. When the composite coating on magnesium alloy is used for a long time, it unavoidably undergoes mechanical or chemical damage. The corrosive medium (such as Cl^-) will inevitably penetrate the coating to reach the substrate surface and oxidize the metallic magnesium into Mg^{2+} ions. Meanwhile, the 8HQ between the polyelectrolyte layer is released and diffused to the magnesium alloy surface along with the corrosive medium. It combines with Mg^{2+} to produce a dense and insoluble $Mg(HQ)_2$ film at the defects, suppressing the corrosion reactions.[58]

Third, there is a sealing effect on the porous structures due to the intrinsic properties of the polyelectrolyte film. Unlike the LDH nanosheets grown perpendicular to the magnesium alloy surface, the polyelectrolyte film was laid over the LDH phase and 8HQ surfaces. This composite structure effectively seals the micro- and nanoscale pores in the LDH film (Scheme 2). Moreover, the polyelectrolyte presents pH buffering and swelling ability, which helps to form a dense barrier layer and reduces the penetration of corrosive media.[27] Compared with the covalent bond, the activation energy required to break the ionic bond of the polyelectrolyte is low. During the exposure process, owing to the fluctuation of local surroundings from aggressive electrolyte to mild condition, partial ionic bonds were broken and then reformed to generate a thermodynamically favorable conformation for these polymer chains, showing mobility and self-healing performance.[37] The detection of both N and S elements evenly distributed in the scratch area in both PEI/PSS/PEI/PSS and PEI/PSS/8HQ/PSS/PEI coatings (Figures 6d, S5, and S6) demonstrates the mobility of the polyelectrolyte at the scratch area.[55] The polyelectrolyte flow effectively seals and repairs the damaged sites (Scheme 2), improving the corrosion protection performance.

Compared with the single LDH layer, the improved corrosion resistance of the PEI/PSS/8HQ/PSS/PEI coating is also related to the reduction of hydrophilicity of the coating surface. Generally, the larger the contact angle of the coating surface, the better the hydrophobicity and the corrosion resistance.[25] The water contact angle (WCA) on the pure LDH layer surface is only 9.5°. This superhydrophilicity (Figure S7a) is consistent with rich hydrophilic −OH groups in the LDH phase. After depositing the polyelectrolyte and 8HQ layers, the WCA value increases significantly to about 50° (Figure S7b−d). The decrease of the surface hydrophilicity of the coating surface agrees with the enhanced corrosion resistance.

4. CONCLUSIONS

The results of this work have demonstrated an effective strategy to construct an 8HQ-sandwiched polyelectrolyte film on an LDH-grown magnesium alloy surface. The LBL self-assembled multilayer polyelectrolyte exhibits superior corrosion protection and a self-healing ability. The strong adhesion of the polyelectrolyte film to the underlying LDH layer effectively seals the micro- and nanoscale pores in the LDH film and reduces the penetration of corrosive media. The mobility characteristics of the polyelectrolyte and the $Mg(HQ)_2$ precipitation generated by the reaction between the inhibitor and oxidized magnesium help to seal and repair the mechanical cracks and defects, effectively suppressing the corrosion processes and reducing the ineffective release and diffusion of 8HQ into the bulk solution. The enhanced longevity of the inhibitor concentration at the substrate surface improves the inhibition durability. The insight into the effective sealing of the micro/nanopores provides a pathway toward designing a long-lasting and highly corrosion-resistant self-healing coating on metal.

■ ASSOCIATED CONTENT

Supporting Information

The Supporting Information is available free of charge at https://pubs.acs.org/doi/10.1021/acsapm.4c00087.

EDS maps of typical elements for different coatings; digital photos of PEI/PSS/8HQ/PSS/PEI coating after scribing; equivalent electrical circuit models; SVET plots of PEI/PSS/8HQ/PSS/PEI composite coating; EDS spectra of coatings at scratches; static contact angles; percentages of different elements, and EIS and Tafel electrochemical parameters of different coatings before and after exposure (PDF)

■ AUTHOR INFORMATION

Corresponding Authors

Zhi-Hui Xie − *Chemical Synthesis and Pollution Control Key Laboratory of Sichuan Province, College of Chemistry and*

https://doi.org/10.1021/acsapm.4c00087
ACS Appl. Polym. Mater. 2024, 6, 4037−4049

Chemical Engineering, China West Normal University, Nanchong 637002, P. R. China; orcid.org/0000-0002-1556-0700; Email: zhxie@cwnu.edu.cn

Chuan-Jian Zhong − *Department of Chemistry, State University of New York at Binghamton, Binghamton, New York 13902, United States;* orcid.org/0000-0003-0746-250X; Email: cjzhong@binghamton.edu

Authors

Wenxi Zhang − *Chemical Synthesis and Pollution Control Key Laboratory of Sichuan Province, College of Chemistry and Chemical Engineering, China West Normal University, Nanchong 637002, P. R. China*

Yanqiu Li − *Chemical Synthesis and Pollution Control Key Laboratory of Sichuan Province, College of Chemistry and Chemical Engineering, China West Normal University, Nanchong 637002, P. R. China*

Qiwen Yong − *Chemical Synthesis and Pollution Control Key Laboratory of Sichuan Province, College of Chemistry and Chemical Engineering, China West Normal University, Nanchong 637002, P. R. China*

Liang Wu − *College of Materials Science and Engineering/ National Engineering Research Center for Magnesium Alloys, Chongqing University, Chongqing 400044, P. R. China;* orcid.org/0000-0002-9988-8593

Xiaoqiang Fan − *Key Laboratory of Advanced Technologies of Materials (Ministry of Education), School of Materials Science and Engineering, Southwest Jiaotong University, Chengdu 610031, P. R. China;* orcid.org/0000-0001-7101-6577

Complete contact information is available at: https://pubs.acs.org/10.1021/acsapm.4c00087

Notes

The authors declare no competing financial interest.

■ ACKNOWLEDGMENTS

This work has been financially supported by the National Natural Science Foundation of China (52271073) and the Sichuan Provincial Natural Science Foundation for Distinguished Young Scholars (2024NSFSC1985). C.-J.Z. acknowledges the support of the National Science Foundation (CHE2102482).

■ REFERENCES

(1) Wu, G.; Chan, K.-C.; Zhu, L.; Sun, L.; Lu, J. Dual-phase nanostructuring as a route to high-strength magnesium alloys. *Nature* **2017**, *545* (7652), 80−83.

(2) Yan, C.; Xin, Y.; Chen, X.-B.; Xu, D.; Chu, P. K.; Liu, C.; Guan, B.; Huang, X.; Liu, Q. Evading strength-corrosion tradeoff in Mg alloys via dense ultrafine twins. *Nat. Commun.* **2021**, *12* (1), No. 4616.

(3) Li, Y.; Ouyang, Y.; Fang, R.; Jiang, X.; Xie, Z.-H.; Wu, L.; Long, J.; Zhong, C.-J. A nickel-underlayer/LDH-midlayer/siloxane-toplayer composite coating for inhibiting galvanic corrosion between Ni layer and Mg alloy. *Chem. Eng. J.* **2022**, *430*, No. 132776.

(4) Rajabalizadeh, Z.; Seifzadeh, D.; Khodayari, A.; Sohrabnezhad, S. Corrosion protection and mechanical properties of the electroless Ni-P-MOF nanocomposite coating on AM60B magnesium alloy. *J. Magnesium Alloys* **2022**, *10* (8), 2280−2295.

(5) Chen, Z.; Scharnagl, N.; Zheludkevich, M. L.; Ying, H.; Yang, W. Micro/nanocontainer-based intelligent coatings: Synthesis, performance and applications − A review. *Chem. Eng. J.* **2023**, *451*, No. 138582.

(6) Huangfu, H.; Guo, X.; Li, N.; Xiong, Y.; Huang, Y.; Zhang, J.; Wang, L. A smart composite coating with self-reporting and self-healing functions to enhance corrosion protection for magnesium alloys. *Prog. Org. Coat.* **2023**, *181*, No. 107598.

(7) Tran, T. H.; Vimalanandan, A.; Genchev, G.; Fickert, J.; Landfester, K.; Crespy, D.; Rohwerder, M. Regenerative nano-hybrid coating tailored for autonomous corrosion protection. *Adv. Mater.* **2015**, *27* (25), 3825−3830.

(8) Wu, Y.; Sun, T.-Y.; Ge, T.; Zhao, W.; Huang, L.-F. Eliminating the galvanic corrosion effect of graphene coating by an accurate and rapid self-assembling defect healing approach. *Adv. Funct. Mater.* **2022**, *32* (13), No. 2110264.

(9) Xiang, T.; Liu, J.; Liu, Q.; Wei, F.; Lv, Z.; Yang, Y.; Shi, Lp.; Li, C.; Chen, D.; Xu, G. Self-healing solid slippery surface with porous structure and enhanced corrosion resistance. *Chem. Eng. J.* **2021**, *417*, No. 128083.

(10) Susarla, S.; Chilkoor, G.; Kalimuthu, J. R.; Saadi, M. A. S. R.; Cui, Y.; Arif, T.; Tsafack, T.; Puthirath, A. B.; Sigdel, P.; Jasthi, B.; Sudeep, P. M.; Hu, L.; Hassan, A.; Castro-Pardo, S.; Barnes, M.; Roy, S.; Verduzco, R.; Kibria, M. G.; Filleter, T.; Lin, H.; Solares, S. D.; Koratkar, N.; Gadhamshetty, V.; Rahman, M. M.; Ajayan, P. M. Corrosion resistance of sulfur−selenium alloy coatings. *Adv. Mater.* **2021**, *33* (51), No. 2104467.

(11) Olivieri, F.; Scherillo, F.; Castaldo, R.; Cocca, M.; Squillace, A.; Gentile, G.; Lavorgna, M. Effectiveness of mesoporous silica nanoparticles functionalized with benzoyl chloride in pH-responsive anti-corrosion polymer coatings. *ACS Appl. Polym. Mater.* **2023**, *5* (8), 5917−5925.

(12) Parulski-Seager, D. C.; Suarez, A.; Getachew, B. A. Monovalent and divalent ions impair recovery of strength when self-healing is facilitated by hydrogen bonding. *ACS Appl. Polym. Mater.* **2023**, *5* (8), 6143−6150.

(13) Shen, T.; Zeng, H.; Chen, Z.; Zhao, S.-R.; Yang, H.-C.; Li, W. Recyclable and self-repairable epoxy anti-corrosion coatings with curing-controlled thermoplasticity. *ACS Appl. Polym. Mater.* **2022**, *4* (2), 1035−1046.

(14) Shao, Z.-B.; Wang, T.-C.; Lin, X.-B.; Song, X.; Cui, J.; Zhang, S.; Zhu, L. Facile construction of inorganic phosphorus/boron-layered double hydroxide complexes for highly efficient fire-safety epoxy resin. *ACS Appl. Polym. Mater.* **2023**, *5* (5), 3768−3776.

(15) Jatav, S.; Herber, M.; Xiang, H.; Hill, E. H. Layered double hydroxide−bismuth molybdate hybrids toward water remediation via selective adsorption of anionic species. *ACS Appl. Mater. Interfaces* **2022**, *14* (46), 51921−51930.

(16) Mohammadi, I.; Shahrabi, T.; Mahdavian, M.; Izadi, M. Construction of an epoxy coating with excellent protection performance on the A.A. 2024-T3 using ion-exchange materials loaded with eco-friendly corrosion inhibitors. *Prog. Org. Coat.* **2022**, *166*, No. 106786.

(17) Ouyang, Y.; Li, L.-X.; Xie, Z.-H.; Tang, L.; Wang, F.; Zhong, C.-J. A self-healing coating based on facile pH-responsive nanocontainers for corrosion protection of magnesium alloy. *J. Magnesium Alloys* **2022**, *10* (3), 836−849.

(18) Tarzanagh, Y. J.; Seifzadeh, D.; Samadianfard, R. Combining the 8-hydroxyquinoline intercalated layered double hydroxide film and sol−gel coating for active corrosion protection of the magnesium alloy. *Int. J. Miner., Metall. Mater.* **2022**, *29* (3), 536−546.

(19) de Luna, M. S.; Buonocore, G. G.; Giuliani, C.; Messina, E.; Di Carlo, G.; Lavorgna, M.; Ambrosio, L.; Ingo, G. M. Long-lasting efficacy of coatings for bronze artwork conservation: The key role of layered double hydroxide nanocarriers in protecting corrosion inhibitors from photodegradation. *Angew. Chem., Int. Ed.* **2018**, *57* (25), 7380−7384.

(20) Rodriguez, J.; Bollen, E.; Nguyen, T. D.; Portier, A.; Paint, Y.; Olivier, M. G. Incorporation of layered double hydroxides modified with benzotriazole into an epoxy resin for the corrosion protection of Zn-Mg coated steel. *Prog. Org. Coat.* **2020**, *149*, No. 105894.

(21) Wang, X.; Li, L.; Xie, Z.-H.; Yu, G. Duplex coating combining layered double hydroxide and 8-quinolinol layers on Mg alloy for corrosion protection. *Electrochim. Acta* **2018**, *283*, 1845−1857.
(22) Shen, S.; Zuo, Y.; Zhao, X. The effects of 8-hydroxyquinoline on corrosion performance of a Mg-rich coating on AZ91D magnesium alloy. *Corros. Sci.* **2013**, *76*, 275−283.
(23) Wu, L.; Chen, Y.; Dai, X.; Yao, W.; Wu, J.; Xie, Z.; Jiang, B.; Yuan, Y.; Pan, F. Corrosion resistance of the GO/ZIF-8 hybrid loading benzotriazole as a multifunctional composite filler-modified MgAlY layered double hydroxide coating. *Langmuir* **2022**, *38* (33), 10338−10350.
(24) Yimyai, T.; Thiramanas, R.; Phakkeeree, T.; Iamsaard, S.; Crespy, D. Adaptive coatings with anti-corrosion and antibiofouling properties. *Adv. Funct. Mater.* **2021**, *31* (37), No. 2102568.
(25) Chen, Y.; Ren, B.; Gao, S.; Cao, R. The sandwich-like structures of polydopamine and 8-hydroxyquinoline coated graphene oxide for excellent corrosion resistance of epoxy coatings. *J. Colloid Interface Sci.* **2020**, *565*, 436−448.
(26) Abu-Thabit, N. Y.; Hamdy, A. S. Stimuli-responsive polyelectrolyte multilayers for fabrication of self-healing coatings − A review. *Surf. Coat. Technol.* **2016**, *303*, 406−424.
(27) Syed, J. A.; Tang, S.; Lu, H.; Meng, X. Smart PDDA/PAA multilayer coatings with enhanced stimuli responsive self-healing and anti-corrosion ability. *Colloids Surf., A* **2015**, *476*, 48−56.
(28) Zhao, Y.-B.; Liu, H.-P.; Li, C.-Y.; Chen, Y.; Li, S.-Q.; Zeng, R.-C.; Wang, Z.-L. Corrosion resistance and adhesion strength of a spin-assisted layer-by-layer assembled coating on AZ31 magnesium alloy. *Appl. Surf. Sci.* **2018**, *434*, 787−795.
(29) Wu, Y.; Wu, L.; Zheludkevich, M. L.; Chen, Y.; Serdechnova, M.; Yao, W.; Blawert, C.; Atrens, A.; Pan, F. MgAl-$V_2O_7^{4-}$ LDHs/(PEI/MXene)10 composite film for magnesium alloy corrosion protection. *J. Mater. Sci. Technol.* **2021**, *91*, 28−39.
(30) Miao, C.; Xun, X.; Dodd, L. J.; Niu, S.; Wang, H.; Yan, P.; Wang, X.-C.; Li, J.; Wu, X.; Hasell, T.; Quan, Z.-J. Inverse vulcanization with SiO_2-embedded elemental sulfur for super-hydrophobic, anti-corrosion, and antibacterial coatings. *ACS Appl. Polym. Mater.* **2022**, *4* (7), 4901−4911.
(31) Dou, B.; Wang, Y.; Zhang, T.; Liu, B.; Shao, Y.; Meng, G.; Wang, F. Growth behaviors of layered double hydroxide on microarc oxidation film and anti-corrosion performances of the composite film. *J. Electrochem. Soc.* **2016**, *163* (14), C917−C927.
(32) Zhang, G.; Wu, L.; Tang, A.; Ma, Y.; Song, G.-L.; Zheng, D.; Jiang, B.; Atrens, A.; Pan, F. Active corrosion protection by a smart coating based on a MgAl-layered double hydroxide on a cerium-modified plasma electrolytic oxidation coating on Mg alloy AZ31. *Corros. Sci.* **2018**, *139*, 370−382.
(33) Chen, Y.; Wu, L.; Yao, W.; Zhong, Z.; Chen, Y.; Wu, J.; Pan, F. One-step in situ synthesis of graphene oxide/MgAl-layered double hydroxide coating on a micro-arc oxidation coating for enhanced corrosion protection of magnesium alloys. *Surf. Coat. Technol.* **2021**, *413*, No. 127083.
(34) Andreeva, D. V.; Skorb, E. V.; Shchukin, D. G. Layer-by-Layer Polyelectrolyte/Inhibitor Nanostructures for Metal Corrosion Protection. *ACS Appl. Mater. Interfaces* **2010**, *2* (7), 1954−1962.
(35) Wang, L.; Zhang, K.; He, H.; Sun, W.; Zong, Q.; Liu, G. Enhanced corrosion resistance of MgAl hydrotalcite conversion coating on aluminum by chemical conversion treatment. *Surf. Coat. Technol.* **2013**, *235*, 484−488.
(36) Zhang, G.; Wu, L.; Tang, A.; Weng, B.; Atrens, A.; Ma, S.; Liu, L.; Pan, F. Sealing of anodized magnesium alloy AZ31 with MgAl layered double hydroxides layers. *RSC Adv.* **2018**, *8* (5), 2248−2259.
(37) Andreeva, D. V.; Fix, D.; Möhwald, H.; Shchukin, D. G. Self-Healing Anti-corrosion Coatings Based on pH-Sensitive Polyelectrolyte/Inhibitor Sandwichlike Nanostructures. *Adv. Mater.* **2008**, *20* (14), 2789−2794.
(38) Zhang, K.; Wang, L.; Liu, G. Copper(II) 8-hydroxyquinolinate 3D network film with corrosion inhibitor embedded for self-healing corrosion protection. *Corros. Sci.* **2013**, *75*, 38−46.
(39) Kim, M.; Hwang, S.; Yu, J.-S. Novel ordered nanoporous graphitic C_3N_4 as a support for Pt−Ru anode catalyst in direct methanol fuel cell. *J. Mater. Chem.* **2007**, *17* (17), 1656−1659.
(40) Yu, S.; Wang, X.; Liu, Y.; Chen, Z.; Wu, Y.; Liu, Y.; Pang, H.; Song, G.; Chen, J.; Wang, X. Efficient removal of uranium(VI) by layered double hydroxides supported nanoscale zero-valent iron: a combined experimental and spectroscopic studies. *Chem. Eng. J.* **2019**, *365*, 51−59.
(41) Cui, Q.; Jiao, G.; Zheng, J.; Wang, T.; Wu, G.; Li, G. Synthesis of a novel magnetic caragana korshinskii biochar/Mg−Al layered double hydroxide composite and its strong adsorption of phosphate in aqueous solutions. *RSC Adv.* **2019**, *9* (32), 18641−18651.
(42) Zhang, Y.; Gao, Z.; Yang, X.; Chang, J.; Liu, Z.; Jiang, K. Fish-scale-derived carbon dots as efficient fluorescent nanoprobes for detection of ferric ions. *RSC Adv.* **2019**, *9* (2), 940−949.
(43) Sarkar, A. K.; Bediako, J. K.; Choi, J.-W.; Yun, Y.-S. Functionalized magnetic biopolymeric graphene oxide with outstanding performance in water purification. *NPG Asia Mater.* **2019**, *11* (1), No. 4.
(44) Mahato, S.; Puigdollers, J.; Voz, C.; Mukhopadhyay, M.; Mukherjee, M.; Hazra, S. Near 5% DMSO is the best: a structural investigation of PEDOT: PSS thin films with strong emphasis on surface and interface for hybrid solar cell. *Appl. Surf. Sci.* **2020**, *499*, No. 143967.
(45) Temperton, R. H.; O'Shea, J. N.; Scurr, D. J. On the suitability of high vacuum electrospray deposition for the fabrication of molecular electronic devices. *Chem. Phys. Lett.* **2017**, *682*, 15−19.
(46) Wang, B.; Li, W.; Liu, Z.; Duan, Y.; Zhao, B.; Wang, Y.; Liu, J. Incorporating Ni-MOF structure with polypyrrole: enhanced capacitive behavior as electrode material for supercapacitor. *RSC Adv.* **2020**, *10* (21), 12129−12134.
(47) Ni, H.; Wang, N.; Yang, Y.; Shen, M.; An, Q.-F. Positively-charged nanofiltration membrane constructed by polyethyleneimine/layered double hydroxide for Mg^{2+}/Li^+ separation. *Desalination* **2023**, *548*, No. 116256.
(48) Jyotheender, K. S.; Srivastava, C. Deposition current density induced alterations in texture and grain boundary constitution of electrodeposited zinc coatings for enhanced corrosion resistance performance. *Metall. Mater. Trans. A* **2023**, *54* (6), 2384−2393.
(49) Singh, A. P.; Srivastava, C. Effect of selective atomic clustering, surface texture and grain boundary constitution on the corrosion behaviour of electrodeposited Sn-xBi coatings. *Corros. Sci.* **2023**, *215*, No. 111039.
(50) Liu, X.; He, H.; Zhang, T. C.; Ouyang, L.; Zhang, Y.-X.; Yuan, S. Superhydrophobic and self-healing dual-function coatings based on mercaptabenzimidazole inhibitor-loaded magnesium silicate nanotubes for corrosion protection of AZ31B magnesium alloys. *Chem. Eng. J.* **2021**, *404*, No. 127106.
(51) Zhu, Y.-X.; Song, G.-L.; Wu, P.-P.; Huang, J.-F.; Zheng, D.-J. A protective superhydrophobic Mg−Zn−Al LDH film on surface-alloyed magnesium. *J. Alloys Compd.* **2021**, *855*, No. 157550.
(52) Sun, W.; Wang, L.; Wu, T.; Pan, Y.; Liu, G. Communication—Multilayer boron nitride nanosheets as corrosion-protective coating fillers. *J. Electrochem. Soc.* **2016**, *163* (2), C16−C18.
(53) Souza, M. E. P.; Ariza, E.; Ballester, M.; Yoshida, I. V. P.; Rocha, L. A.; Freire, C. M. A. Silicone resin to improve corrosion resistance of Zn and ZnFe coated steel. *Matéria (Rio de Janeiro)* **2006**, *11* (1), 16−23.
(54) Hu, T.; Ouyang, Y.; Xie, Z.-H.; Wu, L. One-pot scalable in situ growth of highly corrosion-resistant MgAl-LDH/MBT composite coating on magnesium alloy under mild conditions. *J. Mater. Sci. Technol.* **2021**, *92*, 225−235.
(55) Syed, J. A.; Meng, X. Intelligent Anti-Corrosion Saline-Enabled Self-Healing Polyelectrolyte Multilayer Coatings. In *Advances in Smart Coatings and Thin Films for Future Industrial and Biomedical Engineering Applications*; Makhlouf, A. S. H.; Abu-Thabit, N. Y., Eds.; Elsevier, 2020; pp 207−243.
(56) Vaghefinazari, B.; Lamaka, S. V.; Blawert, C.; Serdechnova, M.; Scharnagl, N.; Karlova, P.; Wieland, D. C. F.; Zheludkevich, M. L.

https://doi.org/10.1021/acsapm.4c00087
ACS Appl. Polym. Mater. 2024, 6, 4037−4049

Exploring the corrosion inhibition mechanism of 8-hydroxyquinoline for a PEO-coated magnesium alloy. *Corros. Sci.* **2022**, *203*, No. 110344.
(57) Lin, J. K.; Hsia, C. L.; Uan, J. Y. Characterization of Mg,Al-hydrotalcite conversion film on Mg alloy and Cl^- and CO_3^{2-} anion-exchangeability of the film in a corrosive environment. *Scr. Mater.* **2007**, *56* (11), 927−930.
(58) Liu, S.; Li, Z.; Yu, Q.; Qi, Y.; Peng, Z.; Liang, J. Dual self-healing composite coating on magnesium alloys for corrosion protection. *Chem. Eng. J.* **2021**, *424*, No. 130551.

https://doi.org/10.1021/acsapm.4c00087
ACS Appl. Polym. Mater. 2024, 6, 4037−4049